

# Submillimetre photometry of typical high-redshift radio quasars

Steve Rawlings<sup>1\*</sup>, Chris J. Willott<sup>1</sup>, Gary J. Hill<sup>2</sup>,  
Elese N. Archibald<sup>3</sup>, James S. Dunlop<sup>4</sup> and David H. Hughes<sup>5</sup>

<sup>1</sup> *Astrophysics, Department of Physics, Denys Wilkinson Building, Keble Road, Oxford, OX1 3RH, UK*

<sup>2</sup> *McDonald Observatory, Department of Astronomy, University of Texas at Austin, Austin, TX 78712, USA*

<sup>3</sup> *Joint Astronomy Centre, 660 N. A‘ohōkū Place, University Park, Hilo, Hawaii, 9620, USA*

<sup>4</sup> *Institute for Astronomy, University of Edinburgh, Blackford Hill, Edinburgh, EH9 3HJ, UK*

<sup>5</sup> *Instituto Nacional de Astrofísica, Óptica y Electrónica (INAOE), Apartado Postal 51 y 216, 72000 Puebla, Pue., Mexico*

4 February 2022

## ABSTRACT

We present submillimetre (SCUBA) photometry of a sample of eight high-redshift ( $2.5 \leq z < 3.5$ ) radio quasars from two redshift surveys: the TEXOX-1000, or TOOT, survey; and the 7C Redshift Survey (7CRS). Unlike the powerful high-redshift radio sources observed previously in the submillimetre, these radio sources are typical of those dominating the radio luminosity density of the population. We detect just two of the TOOT/7CRS targets at  $850\ \mu\text{m}$ , and one of these detections is probably due to synchrotron emission rather than dust. The population represented by the other six objects is detected in a statistical sense with their average  $850\ \mu\text{m}$  flux density implying that they are similar to low-redshift, far-infrared-luminous quasars undergoing at most moderate ( $\lesssim 200\ \text{M}_{\odot}\ \text{yr}^{-1}$ ) starbursts. By considering all the SCUBA data available for radio sources, we conclude that positive correlations between rest-frame far-infrared luminosity  $L_{\text{FIR}}$ , 151-MHz luminosity  $L_{151}$  and redshift  $z$ , although likely to be present, are hard to interpret because of subtle selection and classification biases, small number statistics and uncertainties concerning synchrotron contamination and  $K$ -correction. We argue that there is not yet any compelling evidence for significant differences in the submillimetre properties of radio-loud and radio-quiet quasars at high redshift.

**Key words:** galaxies: active – galaxies: evolution – galaxies: formation – galaxies: jets – galaxies: luminosity function, mass function

## 1 INTRODUCTION

The advent of the Submillimetre Common-User Bolometer Array (SCUBA; Holland et al. 1999) camera on the James Clerk Maxwell Telescope (JCMT) opened up the field of submillimetre cosmology. This, and other, instrument/telescope combinations now routinely detect dusty star-forming galaxies at high redshifts, a process greatly aided by the way in which the steep submillimetre spectral index compensates for distance-dependent dimming, so that two objects of similar far-infrared luminosity have similar observed submillimetre flux density if both lie anywhere in the redshift range  $1 \lesssim z \lesssim 10$  (Blain & Longair 1993).

A major problem in understanding how submillimetre

surveys constrain the history of star formation in the Universe is the difficulty of measuring redshifts for the sources of the submillimetre emission. This problem has not yet been solved, with only small ( $< 10$  per cent) fractions of objects in submillimetre-flux-density-limited samples having reliable spectroscopic redshifts (e.g. Blain et al. 2002).

An alternative strategy for studying the cosmic star-formation history is to make targeted submillimetre observations of objects with known redshifts (e.g. Hughes, Dunlop & Rawlings 1997). Powerful radio sources are important targets, not because the amount of star formation associated with them seems likely to be cosmologically significant, but because of two crucial properties: (i) they appear to be associated with galaxies, and also presumably black holes, with a mass distribution with a large mean and a small dispersion (e.g. Jarvis et al. 2001b); and (ii) studies of the physics of

\* Email: s.rawlings1@physics.ox.ac.uk

their extended radio structures allows the calculation of the time since their jet-producing AGN were first triggered (e.g. Blundell & Rawlings 1999). The first property is potentially very useful for determining how physical properties derived from submillimetre observations (e.g. dust mass and star-formation rate) depend on galaxy, or black hole, mass. The second property can be used to constrain models in which starburst and AGN activity are physically related.

The first large study of the submillimetre emission of high-redshift radio sources was made by Archibald et al. (2001). They used SCUBA on the JCMT to make sensitive (to an 850  $\mu\text{m}$  noise level  $\approx 1$  mJy rms) observations of 47 radio galaxies covering the redshift range  $1 < z < 4.5$ . The chief result of their study was a rise in the detection rates of radio sources from  $\approx 15$  per cent at  $z \lesssim 2.5$  to  $\gtrsim 75$  per cent at higher redshifts. They interpreted their results as indicating that the submillimetre luminosity of radio galaxies, and hence physical quantities like dust mass, increases systematically with redshift.

One important limitation of the Archibald et al. (2001) study was that it targeted only radio galaxies and excluded radio quasars<sup>†</sup>. This was largely a practical decision, because it was thought that the bright radio-emitting cores of quasars might produce troublesome synchrotron contamination. The decision could be defended on the basis of the simplest unified scheme (e.g. Antonucci 1993) in which no differences are predicted in the joint distributions of isotropically-emitted quantities like synchrotron low-frequency-radio and dust submillimetre emission. A follow-up study of the submillimetre properties of powerful radio quasars at  $z \sim 1.5$  (Willott et al. 2002a) revealed a significant difference between the submillimetre luminosities of radio-luminosity-matched quasars and galaxies – the quasars are brighter in the submillimetre by a factor  $\geq 2$ , accounting for synchrotron contamination. Willott et al. show that their result can still be accommodated within a unified scheme provided one allows for systematic changes in the properties of the obscuring material with time after the jet-triggering event (e.g. Blundell & Rawlings 1999; Hirst, Jackson & Rawlings 2003) and/or correlations between quasar luminosity and the probability of viewing a given object as a quasar (e.g. as in the ‘receding torus’ model; Lawrence 1991, Simpson 1998).

A second important limitation of the Archibald et al. (2001) study was that it was confined only to the most radio-luminous sources: such objects contribute marginally to the luminosity density of the radio source population and could plausibly be entirely unrepresentative. The main aim of this paper is to establish the submillimetre properties of typical high-redshift radio sources.

In Sec. 2 we describe how a sample of radio sources was selected for SCUBA follow-up, and how these observations

were made. The results of these observations are presented and discussed. In Sec. 3 we use these results to establish the submillimetre properties of typical high- $z$  radio sources, to look for evidence of correlations between far-IR luminosity, radio luminosity and redshift and to compare and contrast these results with those obtained previously by Archibald et al. (2001) and Willott et al. (2002a). Some concluding remarks are made in Sec. 4.

We use J2000.0 positions throughout. The convention for all spectral indices,  $\alpha$ , is that flux density  $S_\nu \propto \nu^{-\alpha}$ , where  $\nu$  is the observing frequency. We assume throughout a low-density,  $\Lambda$ -dominated Universe in which  $H_0 = 70 \text{ km s}^{-1} \text{ Mpc}^{-1}$ ,  $\Omega_M = 0.3$  and  $\Omega_\Lambda = 0.7$ .

## 2 SCUBA OBSERVATIONS OF HIGH-REDSHIFT TOOT AND 7CRS RADIO SOURCES

### 2.1 Selection of SCUBA targets

Our SCUBA targets were chosen from two of the suite of redshift surveys of low-frequency-selected radio sources outlined by Rawlings (2002): namely, (i) the TEXOx-1000, or TOOT, Survey (Hill & Rawlings 2003); and (ii) parts I & II of the 7C Redshift Survey (7CRS<sup>‡</sup>; Willott et al. 2002b). We aimed to focus on the specific region in the 151-MHz radio luminosity  $L_{151}$  versus redshift  $z$  plane illustrated in Fig. 1. By studying objects in the region of intersection of the lightly-shaded horizontal and vertical bands of Fig. 1 we are sensitive to the one dex range in  $L_{151}$  which contributes  $\sim 50$  per cent of the radio luminosity density across the range in cosmic time  $t$  from 1.8 Gyr, at  $z = 3.5$ , to 2.6 Gyr at  $z = 2.5$  (Willott et al. 2001b).

We used the following selection criteria: for TOOT (Hill & Rawlings 2003), the TOOT00 and TOOT08 sub-regions with  $0.1 \leq S_{151}/\text{Jy} < 0.2$ ,  $2.5 \leq z < 3.5$  and (for a preliminary version of the survey)  $R \lesssim 23.5$ , yielding five targets; for 7CRS,  $S_{151}/\text{Jy} > 0.5$  and  $z \geq 2.5$ , yielding four potential targets of which one, 5C6.291, was excluded from our SCUBA target list because, with a 1.3-mm (IRAM) flux density of  $65 \pm 6$  mJy (Steppe et al. 1995), its submillimetre emission is clearly dominated by a bright synchrotron-emitting core. All objects are radio quasars: for the TOOT sub-sample this is probably because any radio galaxies meeting the  $S_{151}$  and  $z$  criteria would be too faint optically to meet the  $R$  selection criterion; for 7CRS it is because there are no spectroscopically-confirmed radio galaxies in the target region, and none of the few objects without secure redshifts are likely to be at suitably high redshift (Willott, Rawlings & Blundell 2001a). Basic data on the combined TOOT/7CRS sample can be found in Table 1.

<sup>†</sup> We will use the term radio quasar to refer to lobe-dominated steep-spectrum radio sources associated with quasar nuclei. These are the dominant population of radio-loud quasars in the low-frequency-selected samples considered in this paper, whereas compact flat-spectrum quasars can dominate in high-frequency-selected samples. Unified schemes (e.g. Antonucci 1993) invoke an optically-thick obscuring torus which hides the quasar nucleus when the jet axis makes a large angle with the line-of-sight, and such objects are termed radio galaxies.

<sup>‡</sup> Parts I & II of the 7CRS were pursued in regions of the sky covered previously by the 5C radio surveys and, for consistency with previous papers, we use the 5C names throughout.

<sup>¶</sup> We deem an object to be hyperluminous if, after making the corrections for synchrotron contamination detailed in Table 2, it has a far-infrared (30 – 1000  $\mu\text{m}$ ) luminosity  $L_{\text{FIR}} > 10^{13} L_\odot$ ; such objects have a rest-frame infrared (1 – 1000  $\mu\text{m}$ ) luminosity  $L_{\text{IR}} \gg 10^{13} L_\odot$  and, assuming a starburst heats the dust, a star-formation rate  $SFR \gtrsim 1000 M_\odot \text{ yr}^{-1}$  (see Fig. 3). The nine hyper-

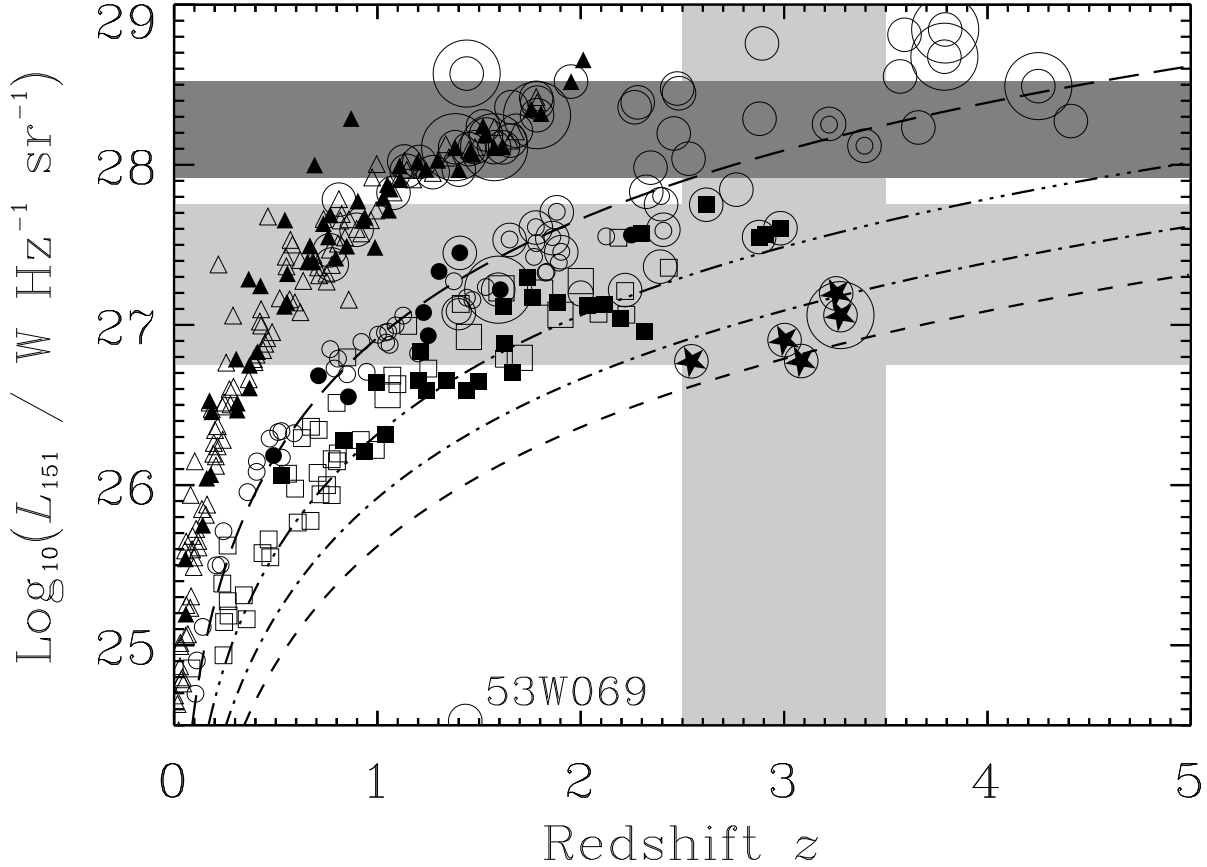


**Figure 1.** The 151-MHz radio luminosity  $L_{151}$  versus redshift  $z$  plane for various complete redshift surveys of radio sources, details of which can be found in the following references: the 3CRR, revised 3C, sample (triangles) – Laing, Riley & Longair (1983); the 6CE sample (circles) – Rawlings, Eales & Lacy (2001); the 7CRS, 7C Redshift Survey (squares) – Willott et al. (2002b); five objects from the TOOT survey (stars) – Hill & Rawlings (2003). Objects classified as radio quasars, following the prescription of Willott et al. (1998), are shown as filled symbols; radio galaxies are shown as open symbols, and these have slightly larger size in the few cases where the redshifts are non-spectroscopic. The intersection of the lightly-shaded horizontal and vertical bands is the region of this plane [ $2.5 \leq z < 3.5$  and  $26.75 \leq \log_{10}(L_{151}) < 27.75$ ] central to the work of this paper. The darkly-shaded band shows the strip in radio luminosity considered in detail by Archibald et al. (2001). The dashed curves show the loci of objects with  $\alpha_{\text{rad}} = 1$  and  $S_{151} = 0.1$  Jy (bottom curve),  $S_{151} = 0.2$  Jy (lower middle curve),  $S_{151} = 0.5$  Jy (upper middle curve) and  $S_{151} = 2.0$  Jy (top curve). Large rings represent hyperluminous infrared galaxies associated with powerful radio sources<sup>¶</sup>, with the smaller rings showing all those objects observed, but not necessarily detected, with SCUBA (Archibald et al. 2001; Willott et al. 2002b; this paper); note that this includes objects, like the very-low- $L_{151}$  object 53W069 (labelled), not in the complete redshift surveys.

## 2.2 SCUBA photometry and origin of the submillimetre emission

The sample of TOOT/7CRS radio sources was observed in photometry mode with the SCUBA bolometer array at the JCMT on the nights 2001 February 24–26, and 2001 July 30–31. Observations were made simultaneously at 850  $\mu\text{m}$  and 450  $\mu\text{m}$ . Our aim was to reach an rms sensitivity of  $\sim 1$  mJy at 850  $\mu\text{m}$  if no clear ( $> 5\sigma$ ) detection was achieved earlier. The data were reduced using the SURF package, following the same methods as Archibald et al. (2001) and Willott et al. (2002a). The resulting submillimetre flux densities are

luminous objects are: 3C181, 3C298, 3C318, 3C432, 6C1045+3513 (Willott et al. 2002a); 4C60.07, 4C41.17, 8C1435+635 (Archibald et al. 2001); TOOT08.061 (this paper).

given in Table 1. Note that the error bars on the photometry do not include systematic uncertainties in the absolute flux calibration which, from inter- and intra-night variations, we estimate to be  $\approx 15$  and  $\approx 30$  per cent at 850- and 450- $\mu\text{m}$  respectively.

Just two of the eight objects are securely detected at 850  $\mu\text{m}$ , and only one of the eight objects at 450  $\mu\text{m}$ . In Fig. 2 we show the spectral energy distributions (SEDs) of the two detected objects. From the comparison of these SEDs with other well-studied objects, it seems clear that the submillimetre emission of the one object detected at 450  $\mu\text{m}$  (TOOT08.061) is dominated by dust emission. The submillimetre emission from the other detected object (5C6.288) is probably dominated by synchrotron emission, although a significant contribution from dust cannot be ruled out.

We have coadded the 850- and 450- $\mu\text{m}$  flux densi-

Name	Class	$z$	$\log_{10}[L_{151}/$ $\text{W Hz}^{-1}]$	$\log_{10}[L_{\text{core}}/$ $\text{sr}^{-1}]$	$M_B$	$D/$ kpc	$S_{850}/$ mJy	$S_{450}/$ mJy
TOOT00_1214	Q(R)	3.084	26.77	$\approx 24.9$	-23.0	$\approx 38^\dagger$	$2.04 \pm 1.18$	$3.8 \pm 11.1$
TOOT00_1261	Q(R)	2.544	26.77	$\approx 24.8$	-22.8	$\approx 24^\dagger$	$1.98 \pm 1.31$	$-18.9 \pm 22.8$
5C6.95	Q(R)	2.877	27.55	25.6	-27.0	119.3	$2.40 \pm 1.23$	$0.3 \pm 13.4$
5C6.288	Q(R)	2.982	27.70	26.8	-24.6	7.7	<b><math>16.74 \pm 1.83</math></b>	$21.6 \pm 22.7$
5C7.70	Q(R)	2.617	27.75	26.3	-25.1	14.4	$0.32 \pm 1.20$	$5.9 \pm 14.8$
TOOT08_061	Q(R)	3.277	27.06	-	-27.1	$< 41.0$	<b><math>8.59 \pm 1.10</math></b>	<b><math>14.9 \pm 5.7</math></b>
TOOT08_079	Q(S)	3.002	26.91	-	-23.7	$< 42.0$	$0.05 \pm 1.14$	$-2.5 \pm 9.1$
TOOT08_094	Q(R)	3.256	27.20	-	-24.1	$< 41.0$	$0.91 \pm 1.05$	$-5.1 \pm 6.5$

**Table 1.** Basic data for the sample observed with SCUBA from Rawlings, Hill & Willott (2004) for the TOOT objects and Willott et al. (1998) for the 7CRS objects. Following the classification scheme of Willott et al. (1998), all objects are quasars, but all show evidence for obscuration. We have therefore sub-divided them according to our best guess as to the nature of the obscuration: Q(R) means the quasar nucleus is seen in lightly-reddened, transmitted light; Q(S) means the quasar nucleus is probably revealed by scattered, rather than transmitted, light – no objects are classified Q(N), meaning a naked quasar nucleus. The absolute  $B$  magnitudes are not corrected for any extinction. Radio core luminosities have been estimated as close as possible to a rest-frame frequency of 5 GHz; a ‘-’ denotes that existing radio data are of too poor resolution to allow isolation of any radio core. A  $\dagger$  denotes that the projected linear size  $D$  is that between the core and an extended component on just one side of the core. The submillimetre photometry comes from the programme described in Sec. 2.2: detections at the  $\geq 2\sigma$  level are given in bold type; no corrections have been made for possible contamination by synchrotron radiation.

ties of the other six targets obtaining an  $\approx 2.5\sigma$  ‘statistical’ detection at  $850\ \mu\text{m}$  given by the variance-weighted mean  $1.22 \pm 0.48$  mJy at  $850\ \mu\text{m}$ , and data consistent with pure noise at  $450\ \mu\text{m}$  (corresponding to a  $2\sigma$  upper limit  $\approx 9$  mJy). Repeating this exercise for just the four TOOT objects without clear submillimetre detections produces similar results ( $1.17 \pm 0.58$  mJy at  $850\ \mu\text{m}$ ), although the significance of the statistical detection at  $850\ \mu\text{m}$  falls to  $\approx 2\sigma$ . We conclude that more TOOT and 7CRS objects would be securely detected at  $850\ \mu\text{m}$  with only slightly deeper photometric observations, although we cannot rule out a ‘bi-modal’ distribution in  $850\text{-}\mu\text{m}$  flux density  $S_{850}$  such that some sources would only be detected with extremely deep exposures.

### 3 THE SUBMILLIMETRE PROPERTIES OF TYPICAL HIGH-REDSHIFT RADIO SOURCES

#### 3.1 Spectral Energy Distributions

We consider first the SED of TOOT08\_061 (Fig. 2), the one TOOT/7CRS object to be detected at both  $450$  and  $850\ \mu\text{m}$ . We used the  $850\ \mu\text{m}$  detection to fix the normalisation of a template quasar SED in the following manner. The model SEDs are the sum of three components: (i) a ‘starburst’ component modelled by an isothermal optically-thin grey body of temperature  $40\ \text{K}$  and emissivity index  $\beta = 2$  (see Priddey & McMahon 2001 for a justification of this choice of parameters); (ii) a ‘Seyfert’ component, dominant at  $3 - 30\ \mu\text{m}$  from Rowan-Robinson (1995); and (iii) a quasar component, dominant in the optical and near-IR, again from Rowan-Robinson (1995). The frequency-integrated luminosities of the three components are fixed in the ratio  $0.3:0.3:1$  so as to reflect the typical values derived by Rowan-Robinson (1995). This SED is consistent with the  $450\ \mu\text{m}$  data point given that it is associated with large random and systematic errors. Accounting for host

galaxy reddening, the model SED also fits well to the optical luminosity of TOOT08\_061. Integrating under the SED, we estimate a bolometric luminosity  $\sim 7 \times 10^{13}\ L_\odot$ , and since the rest-frame infrared ( $1 - 1000\ \mu\text{m}$ ) luminosity  $L_{\text{IR}}$  totals  $\sim 4 \times 10^{13}\ L_\odot$ , TOOT08\_061 is the one object in the TOOT/7CRS sample with sufficient dust emission to classify the object as a hyperluminous infrared galaxy (e.g. Rowan-Robinson 2000).

The correlation between submillimetre luminosity and bolometric luminosity for distant radio quasars (Willott et al. 2002a) makes it no surprise that the brightest submillimetre source in our TOOT/7CRS sample is also the most optically-luminous quasar (see Table 1). The scatter in this correlation means that it is equally unsurprising that the other optically-luminous quasar, 5C6.95, is detected only at the  $\approx 2\sigma$  level with SCUBA.

One guide we have to the more typical properties of high-redshift radio sources comes from an ‘average’ TOOT SED, calculated from simple arithmetic mean values at each frequency, excluding data on TOOT08\_061. This SED, which is clearly biased to a somewhat lower normalisation by the exclusion of TOOT08\_061, is also plotted in Fig. 2. Synchrotron contamination of the  $S_{850} \sim 1$  mJy statistical detection is a slight concern, but, as is illustrated in Fig. 2, extrapolation from radio to sub-mm wavelengths with  $\alpha_{\text{rad}} = 0.7$  [the value for the core of 5C6.288, and seemingly, from the discussion of Willott et al. (2002a), a slightly flatter value than is typical for lobe-dominated radio sources], does not provide a dominant contribution at  $850\ \mu\text{m}$  even if all the NVSS flux density arises from the core. Again fixing the normalisation of a standard quasar SED by the  $S_{850}$  value (Fig. 2), we find consistency with the  $450\ \mu\text{m}$  upper limit and, by integration of the SED, an infrared luminosity  $L_{\text{IR}} \sim 5 \times 10^{12}\ L_\odot$ , dominated presumably by emission from dust.

Accounting for a small amount of dust extinction (amounting to  $A_V = 0.5$  of Milky-Way-type dust as is sufficient to explain the red colours and narrow- $\text{Ly}\alpha$  lines of

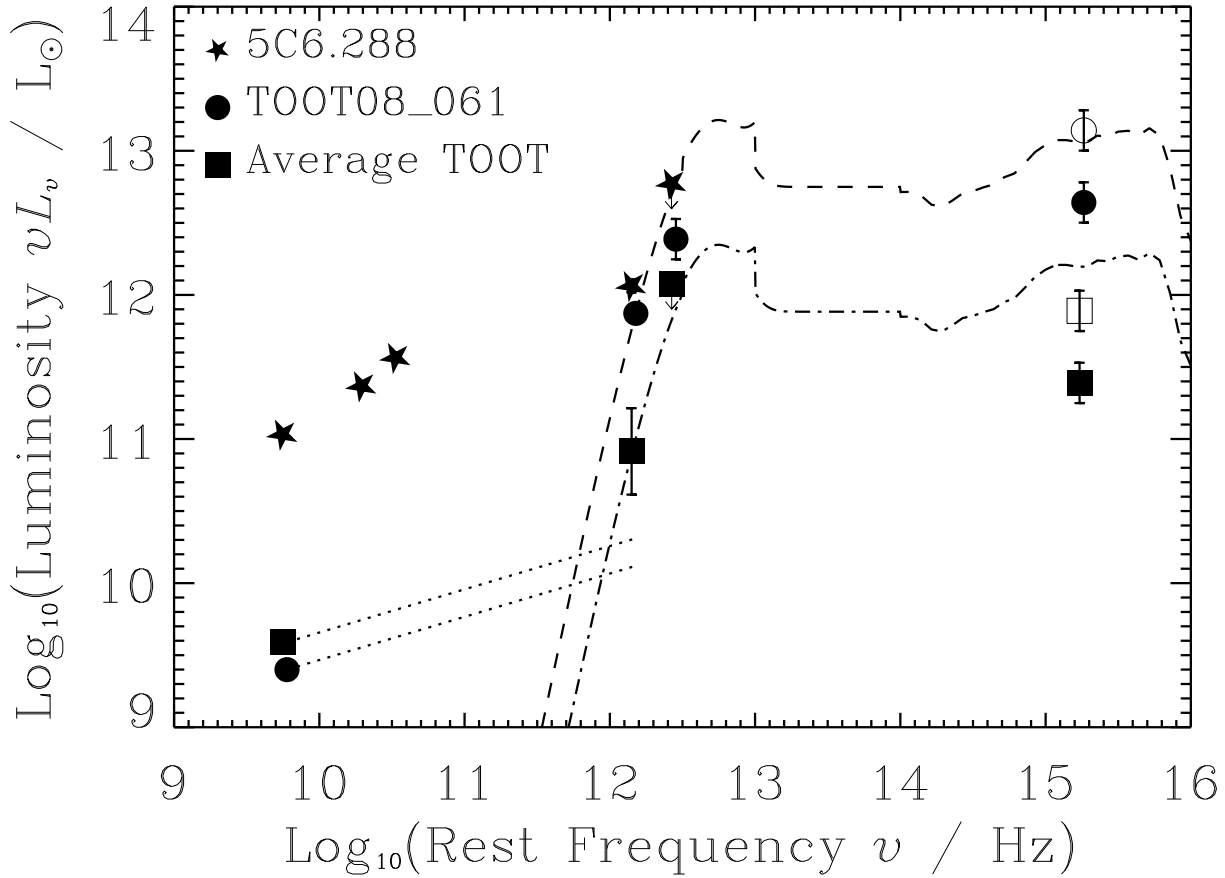


**Figure 2.** The spectral energy distributions (SEDs) of objects in the TOOT/7CRS sample. Data points are shown by the following symbols: TOOT08\_061 (circles); variance-weighted mean of the other four high-redshift TOOT quasars (squares, labelled ‘Average TOOT’); 5C6.288 (stars). Error bars represent just the random errors. Open symbols represent data points corrected for dust extinction (amounting to  $A_V = 0.5$  of Milky-Way-type dust) in the host galaxy. The dotted lines show extrapolations of the radio flux densities assuming a spectral index of 0.7. The dot-dashed lines show model SEDs, normalised to the  $850\ \mu\text{m}$  points, and based on the average quasar SED of Rowan-Robinson (1995) as detailed in Sec. 3.1.

the TOOT quasars; Rawlings et al. 2004), the model SED looks a little too bright at optical wavelengths but, given the crudeness both of the averaging process and the dust extinction correction, the difference between model and data is not very significant. Thus, to the very limited extent to which we can currently define a typical SED for high-redshift TOOT sources, they look similar in shape to those of the low-redshift quasars studied by Rowan-Robinson (1995). The normalisation inferred for the average SED of the TOOT quasars is such that, in terms of infrared luminosity, typical TOOT quasars lie comfortably within the spread exhibited by low-redshift, optically-selected quasars. They are naturally classified alongside low-redshift quasars which have similar far-IR luminosities to ultraluminous infrared galaxies; about one-third of the quasars in optically-selected low-redshift samples have these properties (Rowan-Robinson 1995).

There is of course a continuing debate as to whether star formation or an AGN dominates the heating of the dust responsible for the far-infrared emission from ultraluminous infrared quasars. We can add little to this debate,

noting simply that integration of the average TOOT SED of Fig. 2 gives a rest-frame far-infrared ( $30 - 1000\ \mu\text{m}$ ) luminosity  $L_{\text{FIR}} \sim 2 \times 10^{12}\ L_\odot$  which, in the absence of any quasar heating of the cooler dust, corresponds to a less-than-extreme star-formation rate  $SFR \sim 200\ M_\odot\ \text{yr}^{-1}$  (e.g. from equation [1] of Hughes et al. 1997). Given the possibility of quasar heating, this estimate of  $SFR$  should probably be taken as an upper limit.

### 3.2 Correlations with $L_{151}$ and redshift

We have calculated variance-weighted mean values of  $S_{850}$  in various bins of 151-MHz radio luminosity  $L_{151}$  and redshift  $z$  using the 66 radio sources with SCUBA data plotted with the smaller rings in Fig. 1. We eliminated from consideration the two sources whose  $850\ \mu\text{m}$  data are dominated by synchrotron emission (5C6.288 and 6C0902+34), and we made two assumptions concerning synchrotron contamination of the other objects: (i) zero synchrotron contamination at  $850\ \mu\text{m}$  for all objects; (ii) contamination at the levels detailed in the caption of Table 2. These assumptions should

bracket the uncertainties due to synchrotron contamination. Table 2 contains the results of this analysis, and far-infrared luminosities  $L_{\text{FIR}}$  calculated from these results are plotted against redshift  $z$  in Fig. 3.

### 3.2.1 Correlation with $L_{151}$

The baseline in  $L_{151}$  opened up at high redshift by the TOOT/7CRS objects allows us to look directly for a correlation between  $L_{\text{FIR}}$  and  $L_{151}$  at early cosmic epochs. The results of a straight comparison of the eight TOOT/7CRS objects with the six more radio luminous but similar-redshift objects (8C1039+68, MG1016+058, 4C24.28, 4C28.58, 6C0902+34 and 6C1232+39) from the Archibald et al. (2001) study, excluding the two synchrotron-dominated objects (5C6.288 and 6C0902+34), are included in Table 2 and Fig. 3. Over this restricted redshift range ( $2.5 \leq z < 3.5$ ) we see that, despite a one dex difference in average  $L_{151}$ , there is no difference in average  $S_{850}$ . How does this constrain any correlation between  $L_{151}$  and  $L_{\text{FIR}}$ ?

First, we neglect synchrotron contamination and consider the effects of the submillimetre difference between radio quasars and radio galaxies discovered by Willott et al. (2002a). The average value of  $S_{850}$  for the  $z \sim 3$  TOOT/7CRS objects is likely to be biased high by the exclusion of radio galaxies (see Sec. 2.1), and the average  $S_{850}$  for the higher- $L_{151}$   $z \sim 3$  objects biased low by the exclusion of radio quasars (Archibald et al. 2001). We can estimate the relevant bias factors as follows. As the higher- $L_{151}$  sources have similar values of  $L_{151}$  to the radio quasars studied by Willott et al. (2002a), it is reasonable to assume that they have a similar quasar fraction ( $\approx 0.4$ ; Willott et al. 2000) and a similar submillimetre difference (radio quasars being, after correction for synchrotron contamination, a factor  $\sim 3$  brighter than the radio galaxies at  $850 \mu\text{m}$ ), so that the average  $S_{850}$  would be expected to be a factor  $\sim 2$  higher in a genuinely complete sample. For a genuinely complete TOOT/7CRS sample, the average  $S_{850}$  is likely to be lower, but by a smaller factor because the quasar fraction is likely to be similar (Willott et al. 2000) and there will a lower contribution to the average by the excluded objects. Overall, therefore, for  $z \sim 3$  complete samples, the high- $L_{151}$  point in Fig. 3 is expected to be higher than the low- $L_{151}$  point by a factor  $\sim 2$ . This is a similar separation to that seen between the high- and low- $L_{151}$  points at  $z \sim 1$  and  $z \sim 2$  in Fig. 3, and these do not need large corrections for object exclusion because the Willott et al. (2002a) programme ensured that the SCUBA-targeted radio quasars and radio galaxies ended up in roughly the same ratio as the quasar fraction.

We conclude that, although significant only at the  $\sim 2\sigma$  level (see also Sec. 3.2.2), there is evidence for a  $L_{\text{FIR}}-L_{151}$  correlation in Fig. 3. An increase in  $L_{\text{FIR}}$  by a factor  $\sim 2$  as  $L_{151}$  increases by a factor  $\sim 10$  are consistent with a model in which  $L_{\text{FIR}} \propto L_{151}^p$ , provided  $p \lesssim 0.5$ .

If we adopt the synchrotron-corrected values from Table 2, then a somewhat different picture emerges (Fig 3). Most noticeably, there now exists a large (factor  $\sim 10$ ) difference between the high- and low- $L_{151}$  objects at  $z \sim 1$ . Synchrotron corrections have most effect at low redshift because  $850\mu\text{m}$  corresponds to a lower rest-frame frequency, and most of the SCUBA-targeted galaxies are from the

radio-bright 3C survey<sup>||</sup>. This might be interpreted as evidence that we have, if anything, underestimated the strength and slope of the  $L_{\text{FIR}}-L_{151}$  correlation, or alternatively that the (uncertain) synchrotron corrections have been too severe. However, it is also not completely implausible that the synchrotron corrections are not severe enough [although see Willott et al. (2002a) for arguments to the contrary]. If this were the case, most  $850\mu\text{m}$  detections at  $z \sim 1$  could be dominated by synchrotron contamination and the difference in dust submillimetre luminosity between radio quasars and radio galaxies inferred by Willott et al. (2002a) might have to be reduced. The correct interpretation of Fig. 3 might then be that there is little evidence for a  $L_{\text{FIR}}-L_{151}$  correlation at any redshift, but there is a dramatic drop in  $L_{\text{FIR}}$  at  $z \sim 1$  (see Fig 3); we return to this point in Sec. 3.2.2.

### 3.2.2 Correlation with redshift

The similarity between high- $z$  TOOT/7CRS quasars and some low-redshift optically-selected quasars, discussed in Sec. 3.1, suggests we investigate whether there is any direct evidence for the cosmic evolution in the rest-frame far-infrared luminosities  $L_{\text{FIR}}$  of radio sources of ‘typical’ radio luminosity, i.e. across the lightly-shaded horizontal strip in Fig. 1. The results of this investigation are included in Table 2 and Fig. 3.

Again, we start our discussion by adopting the assumption of negligible synchrotron contamination. The evidence for any systematic rise in  $L_{\text{FIR}}$  with redshift is then weak ( $< 2\sigma$ ) and, as was the case for the hints of a correlation between  $L_{\text{FIR}}$  and  $L_{151}$  (Sec. 3.2.1), driven by the low average  $L_{\text{FIR}}$  of the low- $L_{151}$ ,  $z \sim 1$  bin. Mindful of the many biases discussed in Sec. 3.2.1, we conclude that, neglecting corrections for synchrotron contamination, there is no firm evidence for a cosmic rise in  $L_{\text{FIR}}$  for typical radio luminosity sources. As we have already noted in Sec. 3.2.1, adopting the synchrotron-corrected values from Table 2 means that there is much stronger evidence for cosmic evolution in the sense of a dramatic drop in  $L_{\text{FIR}}$  at  $z \sim 1$ .

Evidence for any cosmic rise in  $L_{\text{FIR}}$  for the high- $L_{151}$  sources (Fig. 3), with or without synchrotron correction, is very weak, driven, this time, by a high average  $L_{\text{FIR}}$  in the  $z \sim 4$  bin, a redshift range not yet probed by SCUBA observations of low- $L_{151}$ , i.e. TOOT, sources. There are just three objects (6C\*0032+412, 8C1435+635, 6C\*0140+326) in this bin, all from the Archibald et al. (2001) SCUBA survey, so small number statistics and selection biases are extremely important. These objects are from ‘filtered’, i.e. steep-radio-spectrum-selected, rather than complete-flux-density-limited, samples (8C, Lacy et al. 1994; 6C\*, Jarvis et al. 2001a). For such samples, 6C\* is the only one in which it has been demonstrated that potentially high- $z$  objects have *not* been missed because of low optical emission line strengths (Jarvis et al. 2001a). Given that scaling relations between luminosities in different wavebands are normally positive, the

<sup>||</sup> Note that the method of synchrotron correction adopted by Archibald et al. (2001) tends to set small positive values of  $S_{850}$  of low- $z$ , typically 3C, sources to zero, whilst leaving negative values unchanged. This may result in ‘corrected’ values which are biased low.

Sample	Range in $L_{151}$	SC	$S_{850}$ at $z = 1$	$S_{850}$ at $z = 2$	$S_{850}$ at $z = 3$	$S_{850}$ at $z = 4$
All in Fig. 1	$26.75 \leq L_{151} \leq 27.75$	n	$0.85 \pm 0.43$ (5)	$1.87 \pm 0.35$ (9)	$2.40 \pm 0.44$ (7)	-
		y	$0.12 \pm 0.43$ (5)	$1.69 \pm 0.35$ (9)	$2.40 \pm 0.44$ (7)	-
All in Fig. 1	$27.90 \leq L_{151} \leq 28.50$	n	$2.52 \pm 0.36$ (8)	$2.97 \pm 0.26$ (16)	$2.63 \pm 0.52$ (3)	$5.84 \pm 0.59$ (3)
		y	$1.55 \pm 0.36$ (8)	$1.82 \pm 0.26$ (16)	$2.47 \pm 0.52$ (3)	$5.77 \pm 0.59$ (3)
Archibald et al.	$27.90 \leq L_{151} \leq 28.50$	n	$1.80 \pm 0.41$ (6)	$2.10 \pm 0.30$ (11)	$2.63 \pm 0.52$ (3)	$5.84 \pm 0.59$ (3)
		y	$0.98 \pm 0.41$ (6)	$0.97 \pm 0.30$ (11)	$2.47 \pm 0.52$ (3)	$5.77 \pm 0.59$ (3)
Archibald et al.	All $L_{151}$	n	$0.96 \pm 0.27$ (13)	$1.60 \pm 0.22$ (21)	$2.82 \pm 0.41$ (5)	$7.38 \pm 0.38$ (7)
		y	$0.20 \pm 0.27$ (13)	$0.89 \pm 0.22$ (21)	$2.70 \pm 0.41$ (5)	$7.32 \pm 0.38$ (7)

**Table 2.** Variance-weighted mean values of 850- $\mu\text{m}$  flux density  $S_{850}$  for samples of radio sources covering various ranges of 151-MHz luminosity  $L_{151}$  and redshift  $z$ . These are calculated for both all the SCUBA-observed radio sources shown in Fig. 1 of this paper, and for just those objects in the Archibald et al. (2001) study. Synchrotron-dominated objects (5C6.288 and 6C0902+34) have been excluded from the analysis, and values calculated both with (SC ‘y’) and without (SC ‘n’) synchrotron correction are given. The synchrotron-corrected values are taken from Archibald et al. excepting for the objects from Willott et al. (2002a) and this paper. For the Willott et al. objects, we assumed a radio-to-submillimetre spectral index  $\alpha = 0.7$ , together with other constraints discussed by Willott et al., to estimate the following synchrotron contaminations, expressed as fractions of the observed  $S_{850}$ : 3C181 (0.06); 3C191 (0.30); 3C205 (0.52); 3C268.4 (0.58); 3C270.1 (0.40); 3C280.1 (0.35); 3C298 (0.38); 3C318 (0.00); 3C432 (0.05); 6C0955+3844 (0.00); 6C1045+3513 (0.05). For the TOOT and 7C objects we estimate zero synchrotron contamination because such low- $S_{151}$  objects can only contribute significantly at 850  $\mu\text{m}$  if their radio flux is concentrated in a compact core (see Fig. 2). The redshift bins used were 0.5 – 1.5, 1.5 – 2.5, 2.5 – 3.5 and 3.5 – 4.5. The number of objects involved in calculating each average are given in brackets.

use of samples in which low-emission-line-strength objects have been missed would have the effect of biasing the average  $S_{850}$  value high. Considering just the two 6C\* objects, we see in Fig. 3 no evidence that  $L_{\text{FIR}}$  is any higher at  $z \sim 4$  than at lower redshift. A rise in average  $L_{\text{FIR}}$  only emerges if one adds in the hyperluminous object 8C1435+635. We caution against putting much weight on either this rise, and its lower formal error bar, because the parent (8C) sample does not have a well-defined redshift completeness. It should also be noticed that any  $z \sim 4$  radio quasars are likely to have been missed by all filtered samples, including 6C\*, because their prominent radio cores can mask steep-spectrum extended emission. The inclusion of such objects would tend to increase the average value of  $S_{850}$  (Willott et al. 2002a).

Adopting the assumption of negligible synchrotron contamination, the weakness of any correlations with redshift in Fig. 3 means we should re-examine the seemingly strong evidence for a cosmic rise in  $L_{\text{FIR}}$  from the study of Archibald et al. (2001). Binned data from their study are presented in Table 2 and plotted in Fig. 4. Considering just those objects in the high- $L_{151}$  strip of Fig. 1 we see that, as in Fig. 3, evidence for a cosmic rise comes from just the  $z \sim 4$  bin, and is subject to the same worries concerning small-number statistics and selection biases. It is only by averaging all the Archibald et al. data, regardless of  $L_{151}$ , that a seemingly monotonic rise in  $L_{\text{FIR}}$  with  $z$  emerges (Fig. 4). There are several potential problems with interpreting this correctly. First, there is a strong and systematic increase in the average  $L_{151}$  of objects from the lowest-redshift bin (mean  $L_{151} = 27.5$ ) to the highest-redshift bin (mean  $L_{151} = 28.6$ ): this could account for nearly all of the ‘cosmic’ rise in  $L_{\text{FIR}}$  given a correlation of the form  $L_{\text{FIR}} \propto L_{151}^p$ , with  $p \lesssim 0.5$  as discussed in Sec. 3.2.1. Second, the average value of the  $z \sim 4$  bin is, despite the low formal error bar, calculated from objects drawn from various filtered surveys, and therefore subject to the possible selection biases discussed in Sec. 3.2.1. Third, the reality and magnitude of any cosmic rise in  $L_{\text{FIR}}$  is strongly dependent on the assumed dust template. Our

choice of dust template (dust temperature  $T = 40$  K, emissivity index  $\beta = 2.0$ ) is motivated by fits to the SEDs of distant quasars by Priddey & McMahon (2001). For this template, objects of a given  $L_{\text{FIR}}$  have higher  $S_{850}$  at  $z \sim 4$  than at  $z \sim 1$ , whereas, as illustrated in Figs. 3 and 4, the Archibald et al. choice of dust template ( $T = 40$  K,  $\beta = 1.5$ ) means that at a given  $L_{\text{FIR}}$ ,  $S_{850}$  is virtually independent of redshift. Thus, for a given cosmology and a given dataset, our choice of dust template will always produce less cosmic evolution than the template adopted by Archibald et al. (2001).

It is also worth re-emphasising that the Archibald et al. (2001) study excluded radio quasars. It could be argued that this reduces, or even eliminates, the need for the complicated corrections for biases discussed in the context of Fig. 3 in Sec. 3.2.1. However, radio galaxies will only show the same relationship between  $L_{\text{FIR}}$  and redshift as the total (radio galaxy plus radio quasar) population if the probability of a radio source being classified as radio galaxy is independent of redshift. This is an as yet unproven assumption, and one that does not sit easily with the results of Hirst et al. (2003) and Willott et al. (2002a) which suggest that both the quasar fraction and submillimetre luminosity are functions of radio source age which, in turn, is likely to correlate negatively with redshift (e.g. Blundell & Rawlings 1999).

#### 4 CONCLUDING REMARKS

We have seen in Sec. 3.2.2 that evidence for evolution of the dust properties of radio sources with redshift emerges only with the adoption of the synchrotron-corrected values for  $S_{850}$ , and is confused by the influence of the correlation between  $L_{\text{FIR}}$  and  $L_{151}$  (Sec. 3.2.1). Since these corrections and this correlation are very uncertain, we conclude that, for radio sources, direct observational evidence that  $L_{\text{FIR}}$  rises systematically with redshift is not yet compelling. Although it would be rather surprising if an increase in the dust and

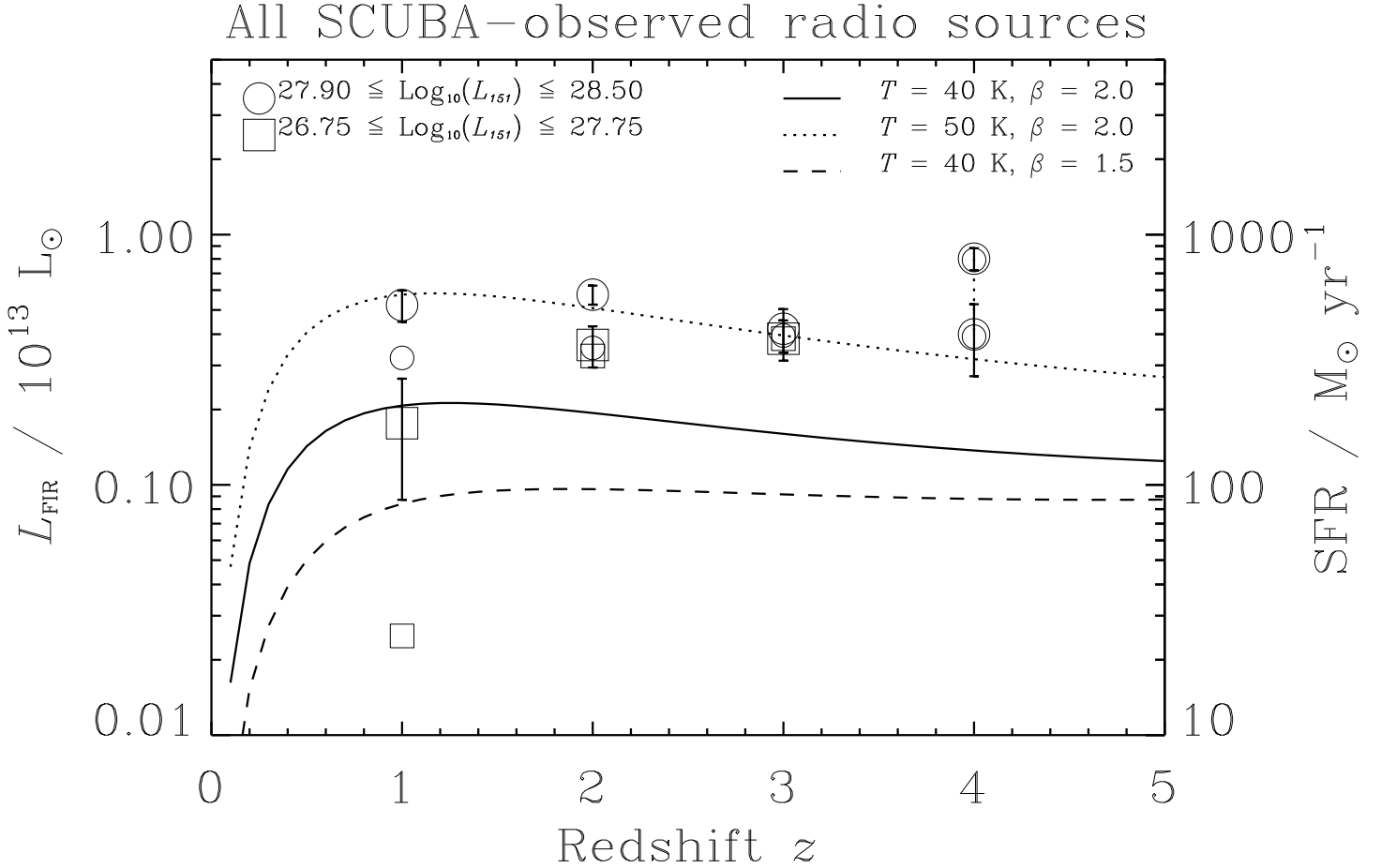


**Figure 3.** The variance-weighted mean far-infrared (30 – 1000  $\mu\text{m}$ ) luminosity  $L_{\text{FIR}}$  of radio sources in selected ranges of 151-MHz luminosity  $L_{151}$  versus redshift  $z$  (in bins 0.5 – 1.5, 1.5 – 2.5, 2.5 – 3.5 and 3.5 – 4.5). All objects identified as observed with SCUBA in Fig. 1, barring three synchrotron-dominated objects, were used to calculate these averages (see Table 2). We have calculated  $L_{\text{FIR}}$  using an isothermal optically-thin grey body spectrum characterised by a temperature  $T = 40\text{ K}$  and emissivity index  $\beta = 2$ ; the locus of an  $S_{850} = 1\text{ mJy}$  source with this spectrum is shown by the solid line, with the effects of varying  $T$  and  $\beta$  being shown by the dotted line ( $T = 50\text{ K}$ ,  $\beta = 2$ ) and the dashed line ( $T = 40\text{ K}$ ,  $\beta = 1.5$ ).  $L_{\text{FIR}}$  is converted to star formation rate  $\text{SFR}$  using eqn. (1) of Hughes et al. (1997), adopting  $\epsilon = 1$ . The large open squares represent radio sources with  $26.75 \leq \log_{10}(L_{151}) < 27.75$ . The large open circles represent radio sources with  $27.9 \leq \log_{10}(L_{151}) < 28.5$ , i.e. the high-luminosity strip considered by Archibald et al. (2001); two different values are plotted at  $z = 4$ , the lower point representing just the two 6C\* objects, the upper point representing all three objects in this bin. The smaller symbols, with error bars not plotted, show the mean values after correction for synchrotron contamination (see Table 2). Note that this plot is affected by the various potential systematic biases discussed in Sec. 3.

gas masses of active galaxies with redshift were not an important part of the overall picture (Archibald et al. 2001), the results of Sec. 3.2 are now in reasonable accord with the results obtained on radio-quiet quasars. Priddey et al. (2003) noted that variations in the submillimetre detectability of optically-selected quasars with redshift are consistent with the K-correction of a template spectrum which does not evolve in normalisation with redshift. Although, submillimetre studies of radio-quiet quasars do not suffer from the problems of synchrotron contamination, it is interesting to note that, for radio-quiet quasars, searches for systematic changes in dust emission with redshift are confused by possible correlations between  $L_{\text{FIR}}$  and optical luminosity (Willott, Rawlings & Grimes 2003; Priddey et al. 2003).

In Sec. 3.2 we have seen that hyperluminous infrared objects contribute substantially to the average values of  $S_{850}$  used in the correlation studies. Looking at the location in

Fig. 5 of the radio-loud objects with associated hyperluminous infrared galaxies hints at complicated physical processes behind any correlations. As has been shown previously by Willott et al. (2002a), and was conjectured by Blundell & Rawlings (1999), there seems to be a clear association of hyperluminous infrared galaxies with the radio sources of smallest projected linear size  $D$ . The underlying physics here (see caption of Fig. 5 for details) may be that a short time  $\tau \lesssim 10^7\text{ yr}$  since the jet-triggering event is a necessary, if not sufficient, condition for far-infrared hyperluminosity as at later times dust may have been destroyed or dispersed by the expanding radio source (De Young 1998). With two important exceptions, the hyperluminous objects appear to be concentrated amongst the most radio-luminous sources. The underlying physics here may be that extreme radio luminosity is strongly linked to the presence of an extreme-luminosity quasar nucleus which in turn promotes, perhaps



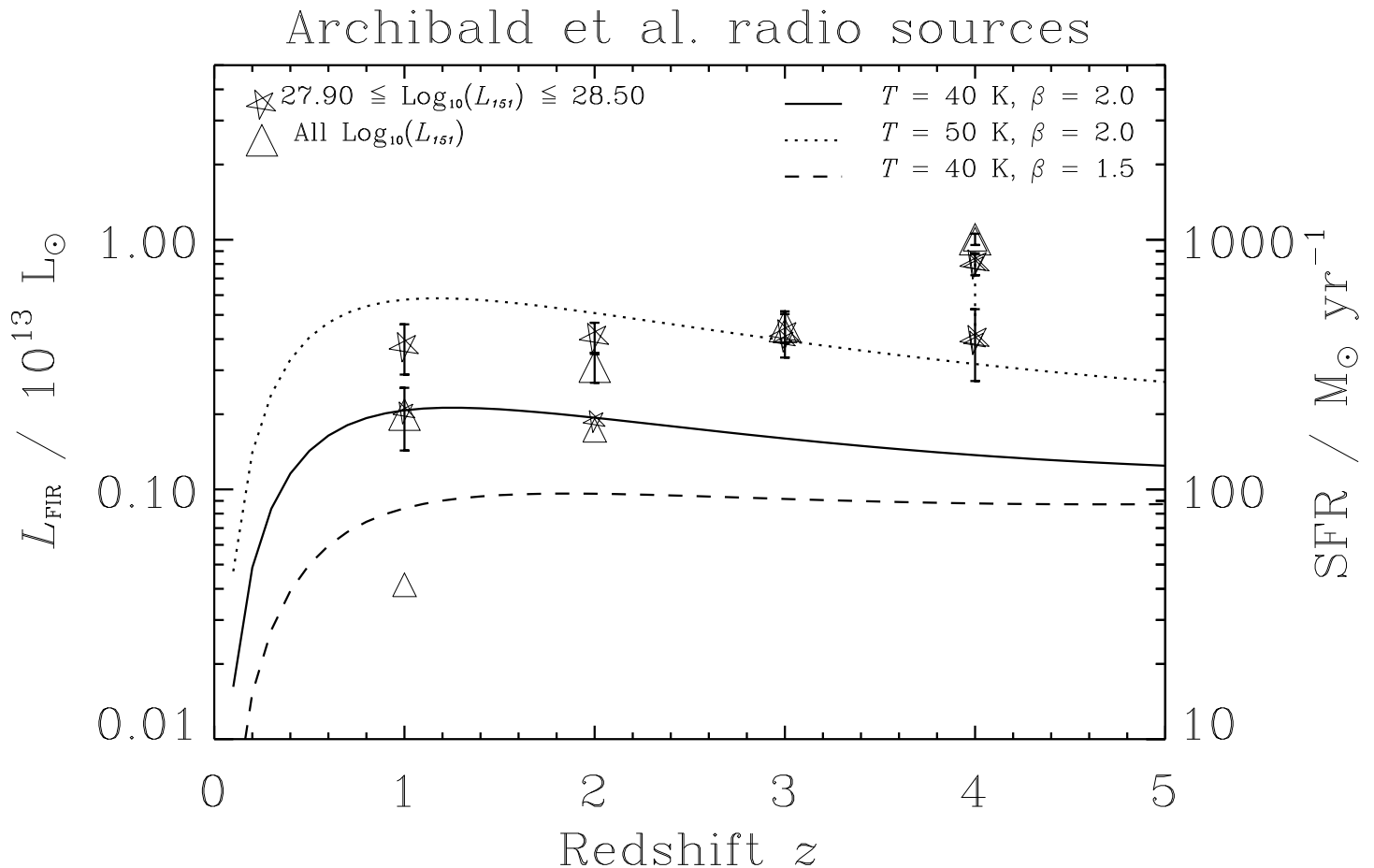


**Figure 4.** The variance-weighted mean far-infrared ( $30 - 1000 \mu\text{m}$ ) luminosity  $L_{\text{FIR}}$  of radio sources in selected ranges of 151-MHz luminosity  $L_{151}$  versus redshift  $z$  (in bins  $0.5 - 1.5$ ,  $1.5 - 2.5$ ,  $2.5 - 3.5$  and  $3.5 - 4.5$ ). Only objects included in the Archibald et al. (2001) study were used to calculate these averages (see Table 2). The axes and lines have the same meaning as in Fig. 3. The large stars represent just the Archibald et al. (2001) objects in the  $27.9 \leq \log_{10}(L_{151}) < 28.5$  strip (two values are plotted at  $z = 4$ , the lower point representing just the two 6C\* objects, the upper point representing all three objects); the large triangles represent all the Archibald et al. (2001) objects, irrespective of radio luminosity. The smaller symbols, with error bars not plotted, show the values after correction for synchrotron contamination (see Table 2). Note that this plot is affected by the various potential systematic biases discussed in Sec. 3.

by direct heating of dust, infrared hyperluminosity. The two hyperluminous objects at relatively low  $L_{151}$  (6C1045+3513 and TOOT08\_061) both show, unusually for radio-loud objects, evidence for broad absorption lines (Willott et al. 2002a; Rawlings et al., 2004). The underlying physics here may be that young bursts of less-than-extreme radio luminosity, probably associated with the early evolution of less powerful jets (e.g. Kuncic 1999), as well as BAL features may be indicative of processes triggered by galaxy mergers (e.g. Canalizo & Stockton 2001).

## ACKNOWLEDGEMENTS

It is our great pleasure to thank Kate Brand and Jonathan Rawlings for their help with the SCUBA observations. Thanks also to Steve Croft, Pamela Gay, Julia Riley, John Swinbank and Joe Tufts for their contributions to the TOOT Survey, and Katherine Blundell and Mark Lacy for their contributions to the 7C Redshift Survey. We also thank the anonymous referee for a very useful report. SR thanks the

PPARC for a Senior Research Fellowship. The JCMT is operated by the Joint Astronomy Centre, on behalf of PPARC, the Netherlands Organisation for Pure Research, and the National Research Council of Canada. This research has made use of the NASA/IPAC Extragalactic Database, which is operated by the Jet Propulsion Laboratory, Caltech, under contract with the National Aeronautics and Space Administration.

## REFERENCES

- Antonucci R.R.J., 1993, ARAA, 31, 473
- Archibald E.N., Dunlop J.S., Hughes D.H., Rawlings S., Eales S.A., Ivison R.J., 2001, MNRAS, 323, 417
- Blain A.W., Longair M.S., 1993, MNRAS, 264, 509
- Blain A.W., Smail I., Ivison R.J., Kneib J.-P., Frayer D.T., 2002, Physics Reports, 369, 111
- Blundell K.M., Rawlings S., 1999, Nature, 399, 330
- Canalizo G., Stockton A., 2001, ApJ, 555, 719
- De Young D.S., 1998, ApJ, 507, 161
- Hill G.J., Rawlings S., 2003, New Astronomy Reviews, 47, 373

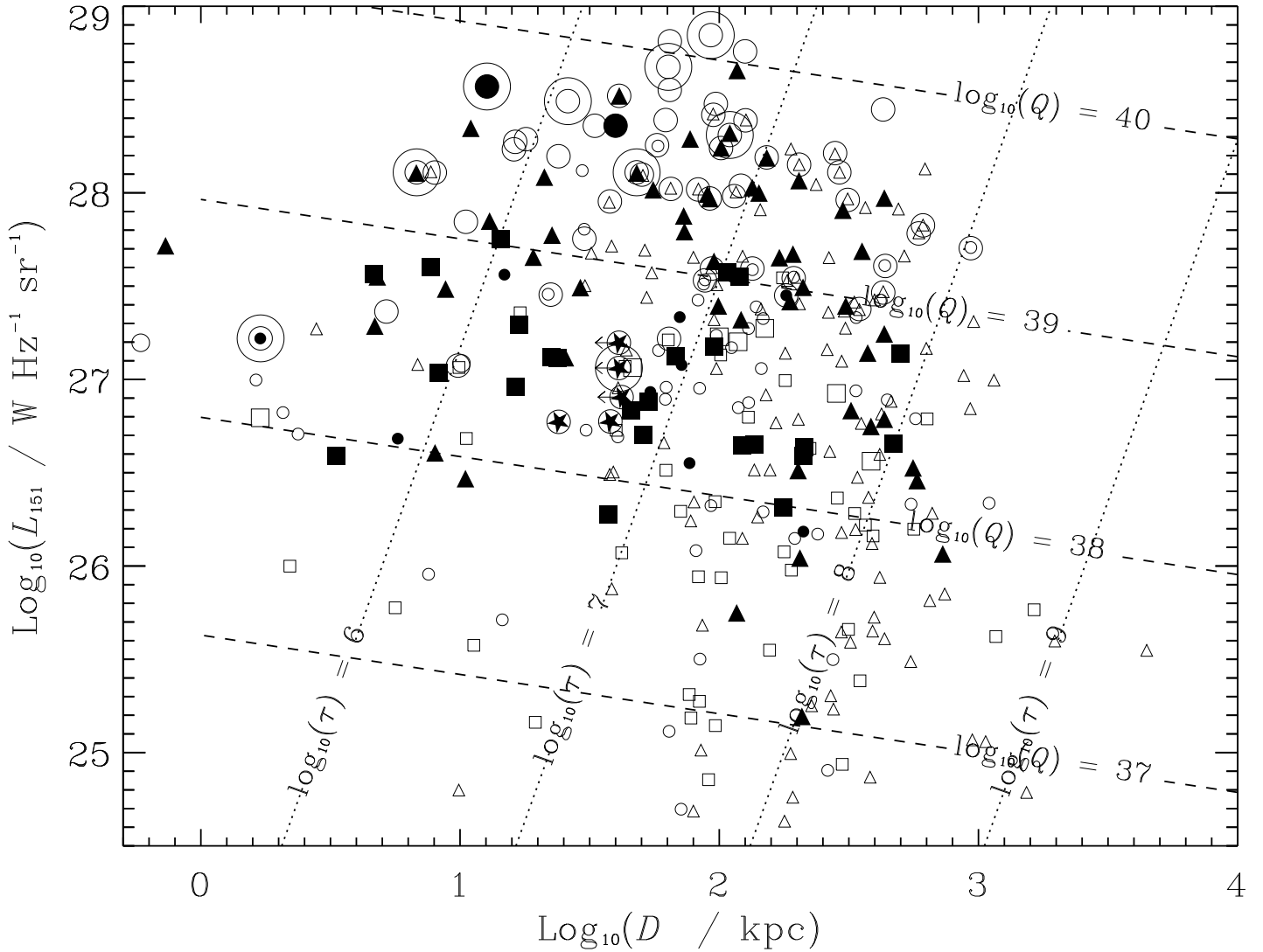


**Figure 5.** The 151-MHz radio luminosity  $L_{151}$  versus projected linear size  $D$  plane for various complete redshift surveys of radio sources (surveys and symbols as in Fig. 1; filled symbols are radio quasars, open symbols are radio galaxies). As in Fig. 1, large rings represent confirmed hyperluminous infrared galaxies and smaller rings represent objects observed with SCUBA, including objects not in the complete redshift surveys. The lines are calculated from the radio source model of Willott et al. (1999) assuming  $\alpha_{\text{rad}} = 1$ : the dotted lines are contours of constant  $\log_{10}(\tau/\text{yr})$ , where  $\tau$  is the time since the jet-triggering event, and the dashed lines are contours of constant  $\log_{10}(Q/W)$ , where  $Q$  is the power in both jets. The values adopted for the fixed parameters of the radio source model (see Willott et al. 1999 for definitions) are as follows:  $\theta = 60^\circ$ ;  $R_T = 5$ ;  $f = 20$ ;  $k = 0$ ;  $\phi = 90^\circ$ ;  $\eta = 1$ ;  $\beta = 1.5$  (here  $\beta$  is the slope of the density power law, not the dust emissivity index);  $c_1 = 2.3$ ;  $n_{100} = 3000 \text{ e}^- \text{ m}^{-3}$ ; none of these parameters, most crucially those of the environment ( $\beta$  and  $n_{100}$ ), are assumed to vary with cosmic time, and some, most notably  $f$ , are sufficiently uncertain that values of  $Q$  and  $\tau$  should be regarded as order-of-magnitude estimates.

Hirst P., Jackson N., Rawlings S., 2003, MNRAS, 346, 1009  
Holland W.S. et al., 1999, MNRAS, 303, 659  
Hughes D.H., Dunlop J.S. & Rawlings S., 1997, MNRAS, 289, 766  
Jarvis M.J. et al., 2001a, MNRAS, 326, 1563  
Jarvis M.J., Rawlings S., Eales S., Blundell K. M., Bunker A. J., Croft S., McLure R. J., Willott C. J., 2001b, MNRAS, 326, 1585  
Kuncic Z., 1999, PASP, 111, 954  
Lacy M. et al., 1994, MNRAS, 271, 504  
Laing R.A., Riley J.M., Longair M.S., 1983, MNRAS, 204, 151

Lawrence A., 1991, MNRAS, 252, 586  
Priddey R.S., McMahon R.G., 2001, MNRAS, 324L, 17  
Priddey R.S., Isaak K. G., McMahon R. G., Omont A., 2003, MNRAS, 339, 1183  
Rawlings, S. 2002, in IAU Symp. 199, The Universe at Low Radio Frequencies, ed. A. P. Rao, G. Swarup & Gopal-Krishna (San Francisco: ASP), p. 34  
Rawlings S., Eales S.A., Lacy M., 2001, MNRAS, 322, 523  
Rawlings S., Hill G.J., Willott C.J., 2004, AJ, to be submitted  
Rowan-Robinson M., 1995, MNRAS, 272, 737  
Rowan-Robinson M., 2000, MNRAS, 316, 885

- Simpson C., 1998, MNRAS, 297, L39  
Willott C.J., Rawlings S., Archibald E.N., Dunlop J.S, 2002a, MNRAS, 331, 435  
Willott C.J., Rawlings S., Blundell K.M., 2001a, MNRAS, 324, 1  
Willott, C.J., Rawlings, S., Blundell, K.M., Lacy, M., Hill, G.J., Scott, S, 2002b, MNRAS, in press  
Willott C.J., Rawlings S., Blundell K.M., Lacy M., 1998, MNRAS, 300, 625  
Willott C.J., Rawlings S., Blundell K.M., Lacy M., 1999, MNRAS, 309, 1017  
Willott C.J., Rawlings S., Blundell K.M., Lacy M., 2000, MNRAS, 316, 449  
Willott C.J., Rawlings S., Blundell K.M., Lacy M. & Eales, S.A., 2001b, MNRAS, 322, 536  
Willott C.J., Rawlings S., Grimes J.A., 2003, ApJ, 598, 909